

1 **Significant Reduction of the Loop Current in the 21st Century and Its Impact**
2 **on the Gulf of Mexico**

3
4
5
6
7
8 Yanyun Liu^{1,2}, Sang-Ki Lee^{1,2}, Barbara A. Muhling^{1,3}, John T. Lamkin³, and David B. Enfield^{1,2}

9 ¹Cooperative Institute for Marine and Atmospheric Studies, University of Miami, Miami,
10 Florida, USA

11 ²Atlantic Oceanographic and Meteorological Laboratory, NOAA, Miami, Florida, USA

12 ³Southeast Fisheries Science Center, NOAA, Miami, Florida, USA

13
14
15 Submitted to Journal of Geophysical Research-Oceans

16 August 2011

17
18
19
20
21
22 Corresponding author address: Yanyun Liu, NOAA/AOML, 4301 Rickenbacker Causeway,
23 Miami, FL 33149, USA. E-mail: Yanyun.Liu@noaa.gov.

1 **Abstract**

2 Here, we examine the potential impact of future anthropogenic global warming on the Gulf
3 of Mexico (GoM) by using a downscaled high-resolution ocean model constrained with the
4 surface forcing fields and initial and boundary conditions obtained from the IPCC-AR4 model
5 simulations under A1B scenario. The simulated volume transport by the Loop Current (LC) is
6 reduced considerably by 20 - 25% during the 21st century, consistent with a similar rate of
7 reduction in the Atlantic Meridional Overturning Circulation. The effect of the LC in the present
8 climate is to warm the GoM, therefore the reduced LC and the associated weakening of the warm
9 LC eddy have a cooling impact in the GoM, particularly in the northern basin. Due to this
10 cooling influence, the northern GoM is characterized as the region of minimal warming. Low-
11 resolution models, such as the IPCC-AR4 models, underestimate the reduction of the LC and its
12 cooling effect, thus fail to simulate the reduced warming feature in the northern GoM. The
13 potential implications of the reduced warming in the northern GoM on pelagic fish species and
14 their spawning patterns are also discussed.

1 **1. Introduction**

2 The IPCC-AR4 climate model simulations under A1B scenario project that the upper ocean
3 temperature in the North Atlantic Ocean may increase by approximately 2°C and the Atlantic
4 Meridional Overturning Circulation (AMOC) may slow down by about 25% during the 21st
5 century [e.g., Schmittner et al. 2005; Drijfhout and Hazeleger. 2006]. Both the increased North
6 Atlantic upper ocean temperature and the decreased AMOC may have strong impacts on the
7 Atlantic marine ecosystem, resulting in substantial reduction of productivity in the Atlantic
8 Ocean owing to reduced upwelling of nutrient-rich deep water and the gradual depletion of
9 upper-ocean nutrient concentration [e.g., Schmittner 2005].

10 Atlantic bluefin tuna (BFT) is one such species that can be greatly affected by future climate
11 change in the Gulf of Mexico (GoM). The spawning of BFT has been recorded predominantly in
12 the northern GoM from April to June (AMJ) with the optimal spawning temperature of 24 - 27°C
13 [e.g., Schaefer 2001]. Adult BFTs are adversely affected by warm water (>28°C) and thus avoid
14 warm features in the GoM such as the Loop Current [Blank et al. 2004]. A recent study, which
15 used the IPCC-AR4 climate model simulations, showed that areas in the northern GoM with high
16 probabilities of larval occurrence could be substantially reduced by the end of the 21st century
17 due to upper ocean temperatures (i.e. temperature at surface, 100m and 200m depth) being
18 outside of the optimal spawning range [Muhling et al. 2011]. BFTs are therefore likely to be
19 vulnerable to climate change, suggesting that there is potential for significant changes in their
20 spawning and migration behaviors.

21 Because the Loop Current (LC) in the GoM is a part of the North Atlantic western boundary
22 currents system and is an important pathway of the AMOC, it is expected that the LC be reduced
23 as the AMOC slows down in the 21st century. Since the advective ocean heat convergence

1 associated with the LC is an important mechanism to offset the surface cooling in the GoM, the
2 reduced LC should play an important role in the projected surface warming in the GoM.
3 However, the IPCC-AR4 climate models have typical spatial resolution of about 1° . As
4 demonstrated by Oey et al. [2005], this is too coarse to properly resolve and estimate the changes
5 in the strength, position and eddy shedding characteristics of the LC. Thus, we use a downscaled
6 high-resolution ocean model to assess the potential impact of future anthropogenic global
7 warming (AGW) on the GoM, with a particular focus on the AMJ, spawning season for BFT.

8

9 **2. Model and Model experiments**

10 The Miami Isopycnic Coordinate Ocean Model (MICOM) version 2.8 is used as the
11 downscaling model in this study. As described in Bleck et al. [1992], the surface mixed layer is
12 modeled by a bulk mixed layer in MICOM, while the turbulent mixing across the mixed layer
13 base is explicitly computed using the turbulence energy equation of Gaspar [1988]. Three new
14 and necessary changes are added to the MICOM. First, the detrainment algorithm is revised
15 following Lee et al. [2007] to suppress spurious warming of the mixed layer induced by
16 detrainment. Second, the shear-driven vertical mixing scheme of Price-Weller-Pinkel (PWP)
17 [Price et al. 1986] is added in such a way that the heat, salt and momentum in the subsurface
18 layer are entrained into the surface mixed layer until satisfying the critical bulk Richardson
19 number of 1.0. Most importantly, the MICOM is coupled with the atmospheric mixed layer
20 model (AML) of Seager et al. [1995], which solves advection-diffusion equations for air
21 temperature and humidity in the planetary boundary layer (PBL). Coupling the MICOM with the
22 AML allows realistic heat and freshwater exchanges at the air-sea interface, and thus prevents
23 the model SSTs from simply damping toward the IPCC-AR4 model SSTs. The air temperature

1 and humidity above the PBL and the wind vector fields in the PBL, which are needed for the
2 coupled MICOM (MICOM-AML), are obtained from the IPCC-AR4 model simulations under
3 20C3M (from 1900 to 2000) and A1B (from 2000 to 2100) scenarios. The initial and boundary
4 conditions are also obtained from the weighted ensembles of the IPCC-AR4 model simulations
5 under the two scenarios as described in the next section.

6 We performed two sets of model experiments, one with a low-resolution MICOM-AML and
7 the other using a version with high resolution. For both experiments, the model domain contains
8 the Atlantic Ocean between 100° W and 20° E bounded north and south by 65° N and 20° S,
9 respectively. The low-resolution model experiment (EXP_LR) has a horizontal resolution of 1°,
10 which is the typical horizontal resolution of the IPCC-AR4 ocean models, and thus cannot fully
11 resolve the strength, position and eddy shedding characteristics of the LC. The high-resolution
12 model (EXP_HR) has the fully eddy-resolving horizontal resolution of 0.1° over the GoM region
13 from 10°N to 30°N and from 100°W to 70°W decreasing linearly to 0.25° in the rest of the model
14 domain.

15 For both the low- and high-resolution configurations, three sets of experiments are conducted
16 for three different periods, namely the late-20th century (from 1981 to 2000), the mid-21st
17 century (from 2041 to 2060) and the late-21st century (from 2081 to 2100). All three sets of
18 experiments are initialized and integrated for 20 years by constraining the MICOM-AML with
19 the surface forcing fields and initial and boundary conditions derived from the IPCC-AR4 model
20 simulations for the corresponding time periods. For each model simulation, the first 10 years of
21 model outputs are discarded to exclude any potentially spurious spin-up effect.

22 In order to minimize the biases in the surface forcing fields obtained from the IPCC-AR4
23 model simulations, we first construct the IPCC-AR4 climatology for the 1971-2000 period, then

1 compute the difference between the IPCC-AR4 climatology and the observed surface forcing
2 climatology - the Coordinated Ocean Research Experiments version-2 (CORE2) surface forcing
3 product [Large and Yeager. 2008] is used to derive the observed surface forcing climatology.
4 Then the difference (i.e., the bias-correction term) is added to the IPCC-AR4 surface forcing
5 fields. The initial and boundary conditions are also bias-corrected following the same
6 methodology used for the surface forcing fields - the observed (U.S. Navy Generalized Digital
7 Environmental Model version 3.0; GDEM3) is used to derive the observed temperature and
8 salinity climatology.

9
10 **3. Weighting the IPCC-AR4 models**

11 Eleven IPCC-AR4 models are used to derive the surface forcing fields and initial and
12 boundary conditions (see Table 1). These eleven IPCC-AR4 models are selected because they all
13 show a realistic AMOC strength in the 20th century and contain all surface flux variables needed
14 for the model experiments. Each of the eleven IPCC-AR4 models is ranked and weighted based
15 on its ability to replicate the observed upper ocean temperature at the surface, 100m and 200m in
16 the GoM for the last 30 years of the 20th century (1971-2000) for AMJ, the major season for
17 BFT spawning. The observed upper ocean temperatures of the 20th century are derived from the
18 GDEM3. Additionally, since the North Atlantic SSTs depend strongly on the AMOC for its
19 effect on the northward advection of warm surface water [e.g., Schmittner, 2005], the AMOC
20 strength based on the maximum overturning streamfunction at 30°N is also used to rank and
21 weight the IPCC-AR4 models. The AMOC strength at 30° N is computed for each IPCC-AR4
22 model during 1971-2000 and compared to the observed value of 18.0 ± 2.5 Sv [Lumpkin and

1 Speer, 2007]. The same weight is given for all four indexes (three temperature levels and
2 AMOC).

3 The weight coefficient is applied to the bias-corrected surface forcing fields and initial and
4 boundary conditions of each IPCC-AR4 model (see Table 1). Then, their weighted ensemble
5 averages are derived and used to perform the MICOM-AML experiments. See Muhling et al.
6 [2011] for detailed description about the weighting of the IPCC-AR4 models. In all model
7 experiments, the ocean boundaries at 65°N and 20°S are treated as closed, but are outfitted with
8 about 5° of buffer zones in which the temperature and salinity are linearly relaxed toward the
9 corresponding IPCC-AR4 fields.

10

11 **4. Results**

12 Figure 1 shows the SST difference in the GoM between the late 21st century and late 20th
13 century in AMJ obtained from the weighted ensemble of IPCC-AR4 models and the MICOM
14 experiments (EXP_LR and EXP_HR). The IPCC-AR4 models show that the GoM is warmed by
15 more than 2°C almost everywhere. The warming is particularly large in the northern GoM, which
16 is the known spawning ground for BFT. This feature in the IPCC-AR4 models is reasonably well
17 reproduced in EXP_LR. Further analysis shows that a subtle imbalance between the downward
18 long-wave radiative flux and the latent heat flux is responsible for the large warming in the
19 northern GoM in both the IPCC-AR4 model composite and EXP_LR (not shown).

20 It is clear that the GoM is also warmed everywhere in EXP_HR, but the spatial pattern of the
21 warming is quite different from the IPCC-AR4 model composite and EXP_LR. In particular, the
22 SST increase in EXP_HR is much less in the northern GoM and a large warming is now
23 confined to the region south of the Florida panhandle. In fact, the northern GoM away from the

1 Florida west coast is now characterized as the region of minimum warming in EXP_HR, whereas
 2 it is a region of maximum warming in both the IPCC-AR4 model composite and EXP_LR. The
 3 projected SST increase over this minimum warming region is only about 1 ~ 1.5°C in EXP_HR,
 4 but it is more than 2°C in EXP_LR. A potential cause for this difference may be the weakening
 5 of the LC and the associated reduction in the warm water transport through the Yucatan Channel,
 6 which are not well simulated in low-resolution models such as the IPCC-AR4 models and
 7 EXP_LR [e.g., Lee et al. 2005; Lee et al. 2007].

8 Figure 2a shows the long-term mean surface current during AMJ in the late 20th century with
 9 a large anticyclone feature in the northern GoM connected to the main branch of the LC. It is
 10 important to note that this feature is visible only in a long-term mean climatology and thus
 11 predominated by transient synoptic eddies in any given time (not shown). Figure 2b shows the
 12 surface current change in the GoM during AMJ between the late 21st century and the late 20th
 13 century. It is clear that the LC is much weakened (note that arrows are reversed from Figure 2a).
 14 It is noticed that an anomalous cyclonic ring (centered around 90°W, 26°N) is formed in the
 15 central and northern GoM. This feature indicates that the warm LC eddy detached from the main
 16 branch of the LC is weakened, and thus shallower (not shown) and colder.

17 To gain a better perspective of how the reduced LC is linked to the reduced warming feature
 18 in the northern GoM in EXP_HR, the surface mixed layer heat budget is diagnosed. The heat
 19 budget equation that governs the diabatic-heating rate in the bulk mixed layer can be written as

$$\underbrace{\rho c_p h_M \frac{\partial T_M}{\partial t}}_{Q_{STR(M)}} = \underbrace{R|_0 + Q_{LAT} + Q_{SEN}}_{Q_{NET}} - \underbrace{\rho c_p \mathbf{v}_M \cdot \nabla T_M}_{Q_{ADV(M)}} - \underbrace{w_e (T_M - T_e)}_{Q_{DIF(M)}}, \quad (1)$$

21 where h_M , T_M , and \mathbf{v}_M are the depth, temperature and velocity vector of the bulk mixed layer,
 22 respectively, w_e is the entrainment rate and T_e is the temperature of an isopycnal layer being

1 entrained. The LHS is the heat storage rate ($Q_{STR(M)}$), the RHS includes the surface net heat flux
2 (Q_{NET}), the advective heat flux convergence ($Q_{ADV(M)}$) and the turbulent heat flux (or entrainment
3 cooling) across the mixed layer base ($Q_{DIF(M)}$), respectively. The advective heat flux convergence
4 term ($Q_{ADV(M)}$) contains only the horizontal component because vertical component does not
5 explicitly contribute to diabatic heating. The horizontal sub-grid diffusion term is ignored
6 because it is small. See Lee et al. [2007] for further discussion on how each term in (1) is related
7 to corresponding term in a slab (i.e., constant depth) mixed layer heat budget equation.

8 Figure 3a and b show the anomalous surface heat flux and advective heat flux convergence in
9 the GoM between the late 21st century and the late 20th century in March, April and May
10 (MAM). Other heat budget terms are not shown because they are much smaller than these two
11 terms. Here, we focus on MAM because of the causal relationship between the heat flux in
12 MAM and the surface mixed layer temperature in AMJ. It is clear that the reduced warming in
13 the northern GoM is largely caused by anomalous advective heat flux divergence associated with
14 the weakened warm LC eddy. The anomalous surface warming is largest in the northern GoM
15 due to the reduced SST warming and reduced latent cooling there (not shown).

16

17 **5. Weakening of the AMOC and the Loop Current**

18 Figure 4a shows the seasonal cycle of the volume transport across the Yucatan Channel for
19 the three different periods obtained from EXP_HR. It is clear that the volume transport is
20 reduced drastically from 24 Sv to 19 Sv, which is about a 25% decrease, by the late 21st century.
21 This is also true for the volume transport through the Florida Straits, the only point of exit from
22 the GoM. The simulated volume transport of 24 Sv in the late 20th century (EXP_HR) agrees
23 reasonably well with the observed estimate of 23.8 ± 1 Sv [e.g., Sheinbaum et al., 2002]. In

1 EXP_LR, the simulated volume transport is only about 9 Sv in the late 20th century, which is
2 unrealistically smaller than the observed estimate, and decreases to 7 Sv by the late 21st century
3 (not shown). As shown in Figure 4b and c, the AMOC is significantly reduced, consistent with
4 Schmittner et al. [2005]. Since the LC is an important pathway of the AMOC, the reduced LC in
5 EXP_HR is likely to be forced remotely by the deceleration of the AMOC. In the next section,
6 we explore how this reduction of the LC in EXP_HR affects the warming of the GoM in the 21st
7 century.

8

9 **6. Cooling effect of the reduced Loop Current**

10 The LC is important for the upper ocean heat budget of the GoM because it carries the warm
11 Caribbean water into the GoM and thus maintains the warmth of GoM. Consistently, the
12 advective flux convergence for the whole column in the GoM during the late 20th century is
13 positive in both EXP_HR (55 TW, $1\text{TW} = 10^{12}\text{W}$) and EXP_LR (25 TW) as summarized in
14 Table 2. Thus, the LC transport in both EXP_HR and EXP_LR has a warming influence to the
15 GoM over the year whereas the net surface flux has a cooling influence over the year and offsets
16 the warming effect by the LC. As shown in Figure 5d, the advective heat flux convergence plays
17 an important role in the GoM in EXP_HR since the LC carries warmer water from Caribbean
18 Sea into the GoM especially in spring and early summer, thus offsetting the surface cooling in
19 GoM during winter.

20 In EXP_LR, on the other hand, the advective heat flux convergence only plays a minor role
21 in the GoM due to unrealistically weak LC. Figures 5b and 5e show the anomalous (i.e., late 21st
22 century – late 20th century) seasonal cycle of heat budget terms averaged in the GoM for
23 EXP_LR and EXP_HR, respectively. The combined effect of anomalous surface flux and

1 advective heat flux convergence results in the warming of GoM. As summarized in Table 2, the
 2 surface flux increases more in EXP_HR (5.0 TW) than that in EXP_LR (3.1 TW), but the
 3 advective heat convergence increases much less in EXP_HR (3.9 TW) than that in EXP_LR (7.3
 4 TW). Particularly from late summer to spring months (September – March), in EXP_HR, the
 5 GoM is subject to anomalous advective heat flux *divergence* (i.e., $\Delta Q_{ADV} < 0$) as shown in Figure
 6 5e. However, in EXP_LR, the GoM is influenced by anomalous advective heat flux *convergence*
 7 (i.e., $\Delta Q_{ADV} > 0$) year-around (Figure 5b).

8 In order to understand how the reduced LC may affect the heat budget of the GoM, it is
 9 important to explore more about the anomalous advective heat convergence (ΔQ_{ADV} , LHS) into
 10 the GoM, which can be given by

$$11 \quad \Delta Q_{ADV} = \underbrace{\rho c_p V \Delta \delta T}_{\Delta Q_{\delta T}} + \underbrace{\rho c_p \Delta V \delta T}_{\Delta Q_V} + \underbrace{\rho c_p \Delta \delta T \Delta V}_{\Delta Q_{\delta T V}}, \quad (2)$$

12 where ρ is the seawater density, c_p is the specific heat of seawater, V is the volume transport
 13 across the Yucatan Channel (or Florida Channel), δT is the temperature difference between the
 14 Yucatan Channel and Florida Straits (i.e., $T_{YUC} - T_{FLO}$), which is always positive, and ΔF
 15 represents the difference in the variable F between the late 21st century and the late 20th century.

16 The LHS is the anomalous advective heat flux convergence (ΔQ_{ADV}). The RHS shows all the
 17 contributing terms of ΔQ_{ADV} (i.e., $\Delta Q_{\delta T}$, ΔQ_V and $\Delta Q_{\delta T V}$). The second term on the RHS of (2),
 18 which is referred to as ΔQ_V , is negative if the LC is reduced (i.e., $\Delta V < 0$). Therefore, the reduced
 19 LC results in anomalous advective heat flux divergence in the GoM, and thus cools the GoM
 20 basin. However, the first term in the RHS, which is referred to as $\Delta Q_{\delta T}$, is positive in both
 21 EXP_HR and EXP_LR and dominates the other term as summarized in Table 3. Therefore, the
 22 GoM is affected by anomalous advective heat flux convergence (i.e., advective warming) during

1 the 21st century. The positive value of $\Delta Q_{\delta T}$ is associated with the increased δT during the 21st
2 century (see equation 2). Thus, the water that enters from the Caribbean Sea warms more than
3 the water that exits through the Florida Straits. The third term is the nonlinear term ($\Delta Q_{\delta TV}$),
4 which is smaller than other two terms.

5 The advective heat budget summarized in Table 3 (for annual mean and Table 4 for MAM
6 season) clearly indicates that the anomalous advective heat flux convergence in the GoM is too
7 high in EXP_LR (7.3 TW in EXP_LR versus 3.9 TW in EXP_HR) because the basin-wide
8 cooling associated with the reduced LC (ΔQ_V) is too small in EXP_LR (-3.5 TW in EXP_LR
9 versus -11.7 TW in EXP_HR).

10 Figure 5c and 5f show the anomalous (i.e., late 21st century – late 20th century) seasonal
11 cycle of advective heat convergence and all the contributing terms ($\Delta Q_{\delta T}$, ΔQ_V and $\Delta Q_{\delta TV}$)
12 averaged in the GoM for EXP_LR and EXP_HR, respectively. The cooling associated with the
13 reduced LC (ΔQ_V) is large and thus plays an important role in EXP_HR, especially in spring and
14 early summer, whereas ΔQ_V in EXP_LR is much smaller and thus not an important player,
15 clearly explaining why the GoM is warmed more in EXP_LR than in EXP_HR. In other words,
16 the cooling associated with the reduced LC (ΔQ_V) is underestimated in EXP_LR because the LC
17 reduction during the 21st century is only 1.6 Sv in EXP_LR, whereas it is 4.7 Sv in EXP_HR.

18

19 **7. Summary and Discussions**

20 In this paper, we examine the potential impact of future AGW on the GoM by using a high-
21 resolution MICOM-AML constrained with the surface forcing fields and initial and boundary
22 conditions obtained from the IPCC-AR4 model simulations under A1B scenario. The LC
23 transport has a net warming influence on the GoM, whereas the net surface flux has a net cooling

1 influence and thus offsets the warming influence of the LC. The simulated volume transport
2 across the Yucatan Channel (and the Florida Channel) is reduced by 20 - 25% during the 21st
3 century, consistent with a similar rate of reduction in the AMOC. The reduced LC and the
4 associated weakening of the warm LC eddy have a cooling impact in the GoM, particularly in
5 the northern GoM. Therefore, the northern GoM where LC eddies predominate is characterized
6 as the region of minimal warming. Low-resolution models, such as the IPCC-AR4 models,
7 underestimate the reduction of the LC and its cooling effect, thus fail to simulate the reduced
8 warming feature in the northern GoM.

9 The reduced warming in the northern GoM will have important implications for marine
10 ecosystems, including the spawning of BFT in AMJ. Since the spawning of BFT is mainly
11 temperature dependent and BFT are adversely affected by warm water, the reduced warming in
12 the northern GoM will probably mitigate the IPCC-projected reduction in the areas of BFT
13 spawning ground in the GoM [Muhling et al. 2011]. Therefore, it is essential to utilize
14 downscaled models and reevaluate the potential effects of climate change on the spatial and
15 temporal extent of BFT spawning in the GoM.

16 Finally, it is important to point out some of the limitations in this study. Here, we mainly
17 focused on the temperature change in the GoM. Other factors including the salinity, the position
18 and eddy-shedding process of LC should also be studied in detail in the future. Further research
19 is also required on the ecosystem based-responses to climate changes in the GoM. This study
20 will also benefit from the development of regional coupled atmosphere-ocean models.

21

1 **Acknowledgements.** This work was supported by grants from the National Oceanic and
2 Atmospheric Administration and National Science Foundation, and a grant from the National
3 Aeronautics and Space Administration.

4

5 **References.**

- 6 Blank, J. M., J. M. Morrisette, A. M. Landeira-Ferandez, S. B. Blackwell, T. D, Williams, and
7 B. A. Block (2004), In situ cardiac performance of Pacific bluefin tuna hearts in response to
8 acute temperaturechange. *J.Exp Biol*, 207, 881–890.
- 9 Bleck, R., C. Rooth, D. Hu, and L. T. Smith, (1992), Salinity-driven thermocline transients in a
10 wind- and thermohaline-forced isopycnic coordinate model of the North Atlantic. *J. Phys.*
11 *Oceanogr.*, **22**, 1486–1505.
- 12 Drijfhout, S. S., and W. Hazeleger, (2006), Changes in MOC and gyre-induced Atlantic Ocean
13 heat transport. *Geophys. Res. Lett.*, **33**, L07707, doi:10.1029/2006GL025807.
- 14 Gaspar, P., (1988), Modeling the seasonal cycle of the upper ocean. *J. Phys. Oceanogr.*, 18, 161-
15 180.
- 16 Large, W.G. and S.G. Yeager, (2008), The Global Climatology of an Interannually Varying Air-
17 Sea Flux Data Set. *Clim. Dyn.*, doi:10.1007/s00382-008-0441-3.
- 18 Lee, S.-K., D. B. Enfield, C. Wang, (2005), Ocean General Circulation Model Sensitivity
19 Experiments on the Annual Cycle of Western Hemisphere Warm Pool. *J. Geophys. Res.*,
20 110, doi:10.1029/2004JC002640.
- 21 Lee, S.-K., D. B. Enfield, C. Wang, (2007), What Drives Seasonal Onset and Decay of the
22 Western Hemisphere Warm Pool? *J. Climate*, 20, 2133-2146.

1 Lumpkin, R., and K. Speer, (2007), Global Ocean Meridional Overturning. *J. Phys. Oceanogr.*,
2 37, 2550–2562.

3 Muhling, B. A., S-K Lee., J. T. Lamkin, and Y. Liu, (2011), Predicting the effects of climate
4 change on bluefin tuna (*Thunnus thynnus*) spawning habitat in the Gulf of Mexico. – *ICES J.*
5 *Mar. Sci.*, doi:10.1093/icesjms/fsr008.

6 Oey, Lie-Yauw, Tal Ezer, and H C Lee, (2005), Loop Current, rings and related circulation in the
7 Gulf of Mexico: A review of numerical models and future challenges. *In Circulation in the*
8 *Gulf of Mexico: Observations and Models*, Washington, DC, AGU, 31-56.

9 Price, R., A. Weller, and R. Pinkel (1986), Diurnal cycling: Observations and models of the
10 upper ocean response to diurnal heating, cooling, and wind mixing. *J. Geophys. Res.*, 91,
11 8411–8427.

12 Schaefer, K.M. (2001), Reproductive biology. In: *Tunas: Physiology, ecology and evolution* B.A.
13 Block, E.D. Stevens (eds). San Diego, California: Academic Press. pp. 225-270.

14 Schmittner, A., (2005), Decline of the marine ecosystem caused by a reduction in the Atlantic
15 overturning circulation. *Nature*, 434, 628-633.

16 Schmittner, A., M. Latif, B. Schneider, (2005), Model Projections of the North Atlantic
17 thermohaline circulation for the 21st century assessed by observations *Geophys. Res. Lett.*,
18 32, L23710, doi:10.1029/2005GL024368.

19 Seager, R., M.B. Blumenthal, and Y. Kushnir, (1995), An Advective Atmospheric Mixed Layer
20 Model for Ocean Modeling Purposes: Global Simulation of Surface Heat Fluxes. *J. Climate*,
21 8, 1951–1964.

22 Sheinbaum, J., J. Candela, A. Badan, and J. Ochoa, (2002): Flow structure and transport in
23 Yucatan Channel, *Geophys. Res. Lett.*, 29 (3), 1040, doi:10.1029/2001GL013990.

1 **Figure Captions**

2 **Figure 1.** SST difference in the GoM between the late 21st century and late 20th century during
3 AMJ obtained from (a) the weighted ensemble of 11 IPCC-AR4 models, (b) the low-resolution
4 MICOM experiment (EXP_LR) and (c) the high-resolution MICOM experiment (EXP_HR).

5
6 **Figure 2.** (a) Long-term mean surface current in the late 20th century during AMJ obtained from
7 EXP_HR. (b) Anomalous (i.e., late 21st century – late 20th century) surface current in the GoM
8 during AMJ obtain from EXP_HR.

9
10 **Figure 3.** (a) Anomalous (i.e., late 21st century – late 20th century) surface heat flux in the GoM
11 during MAM obtained from EXP_HR. (b) Anomalous (i.e., late 21st century – late 20th century)
12 advective heat flux convergence (colored) and surface current (vector) in the GoM during MAM
13 obtained from EXP_HR. The unit for the heat flux terms is W/m^2 .

14
15 **Figure 4.** (a) Seasonal cycle of the volume transport (Sv) across the Yucatan Channel for three
16 different periods (the late 20th century, the mid 21st century and the late 21st century) obtained
17 from EXP_HR. Time-averaged Atlantic MOC in (b) the late 20th century and (c) the late 21st
18 century obtained from EXP_HR.

19
20 **Figure 5.** Seasonal cycle of heat budget terms averaged in the GoM (a) for EXP_LR in the late
21 20th century and (d) EXP_HR in the 20th century. Anomalous (i.e., late 21st century – late 20th
22 century) seasonal cycle of heat budget terms averaged in the GoM (b) for EXP_LR and (e)
23 EXP_HR. Anomalous (i.e., late 21st century – late 20th century) seasonal cycle of advective heat

1 convergence and all the contributing terms ($\Delta Q_{\delta T}$, ΔQ_V and $\Delta Q_{\delta TV}$) averaged in the GoM (c) for
2 EXP_LR and (f) EXP_HR.

3

4

5

6

7

8

9

10

11

12

13

14

15

16

17

18

19

20

21

22

1 Table 1. The weight of each IPCC-AR4 model used to derive the surface flux fields and initial
2 and boundary conditions for the MICOM-AML simulations.

Rank	Model	Model Weight
1	CSIRO_MK3_5	1.67
2	MRI_CGCM2_3_2A	1.50
3	GISS_MODEL_E_R	1.17
4	MPI_ECHAM5	1.07
5	NCAR_CCSM3	1.02
6	GFDL_CM2_1	1.00
7	MIROC3_2_MEDRES	0.94
8	MIUB_ECHO_G	0.88
9	GISS_AOM	0.86
10	GFDL_CM2_0	0.70
11	IPSL_CM4	0.17

3
4
5
6
7
8
9
10
11

1 Table 2. Annual heat budget terms (Q_{NET} : surface heat flux; Q_{ADV} : advective heat flux
 2 convergence; and Q_{STR} : heat storage rate) averaged in the GoM for the late 20th century, the late
 3 21st century and the difference between the two periods obtained from EXP_HR and EXP_LR.

Period Experiment	Late 20C (EXP_HR)	Late 21C (EXP_HR)	Difference (EXP_HR)	Late 20C (EXP_LR)	Late 21C (EXP_LR)	Difference (EXP_LR)
Q_{NET}	-54.6	-49.6	5.0	-24.4	-21.4	3.1
Q_{ADV}	54.9	58.8	3.9	24.9	32.2	7.3
Q_{STR}	0.3	9.2	8.9	0.5	10.9	10.4

4
5
6
7
8
9
10
11
12
13
14
15
16
17
18

1 Table 3. Anomalous advective heat flux convergence ΔQ_{ADV} in the GoM and all the contributing
 2 terms in the EXP_HR and EXP_LR experiments. $\Delta \delta T$ is the temperature difference between the
 3 Yucatan Channel and Florida Straits (i.e., $T_{YUC} - T_{FLO}$) in the late 21st century minus that during
 4 the late 20th century, and ΔV is volume transport change between the late 20th and the 21st
 5 century. The unit for the heat flux terms is TW.

Experiment	ΔQ_{ADV}	$\Delta Q_{\delta T}$	ΔQ_V	$\Delta Q_{\delta TV}$	$\Delta \delta T$ ($^{\circ}\text{C}$)	ΔV (Sv)
EXP_HR	3.9	19.5	-11.7	-3.9	0.26	-4.70
EXP_LR	7.3	12.5	-3.5	-1.7	0.34	-1.60

6
7
8
9
10
11
12
13
14
15
16
17
18
19
20

1 Table 4. Anomalous advective heat flux convergence ΔQ_{ADV} in the GoM and all the contributing
2 terms in the EXP_HR and EXP_LR experiments during MAM season.

Experiment	ΔQ_{ADV} (TW)	$\Delta Q_{\delta T}$ (TW)	ΔQ_V (TW)	$\Delta Q_{\delta TV}$ (TW)
EXP_HR	15.8	43.8	-18.8	-9.3
EXP_LR	18.1	25.7	-4.6	-2.9

3
4
5
6
7
8
9
10
11
12
13
14
15
16
17
18
19
20

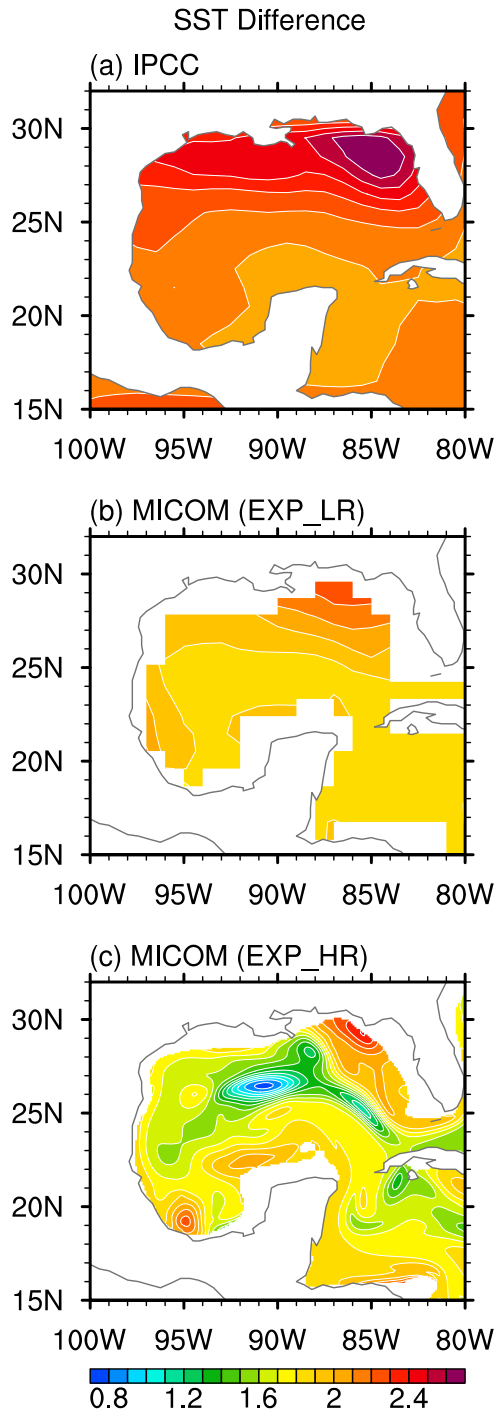


Figure 1. SST difference in the GoM between the late 21st century and late 20th century during AMJ obtained from (a) the weighted ensemble of 11 IPCC-AR4 models, (b) the low-resolution MICOM experiment (EXP_LR) and (c) the high-resolution MICOM experiment (EXP_HR).

MICOM (EXP_HR): Surface Current

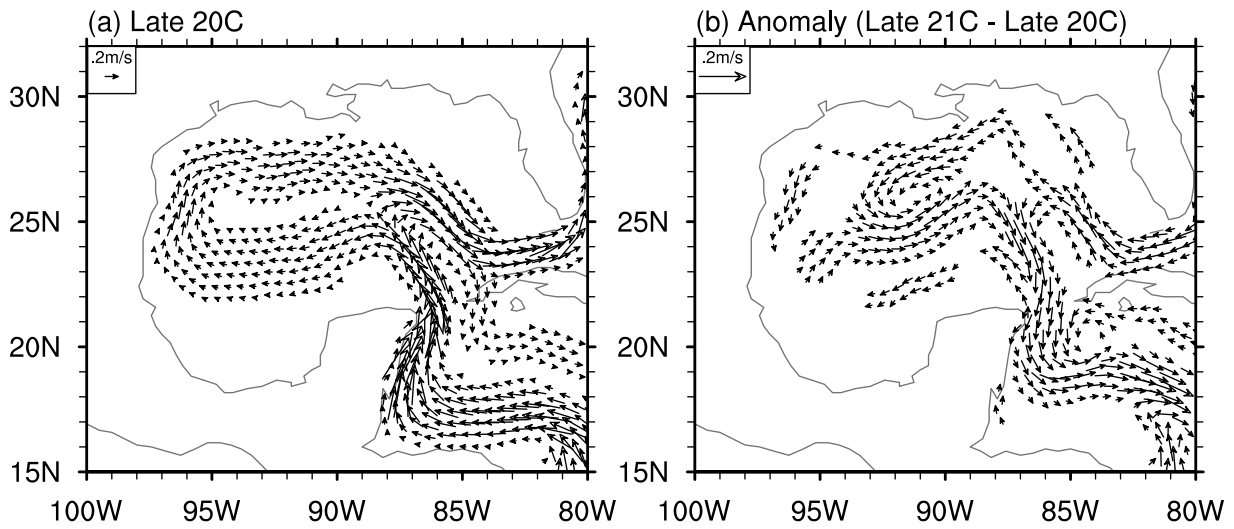


Figure 2. (a) Long-term mean surface current in the late 20th century during AMJ obtained from EXP_HR. (b) Anomalous (i.e., late 21st century – late 20th century) surface current in the GoM during AMJ obtain from EXP_HR.

MICOM (EXP_HR): Mixed Layer Heat Budget

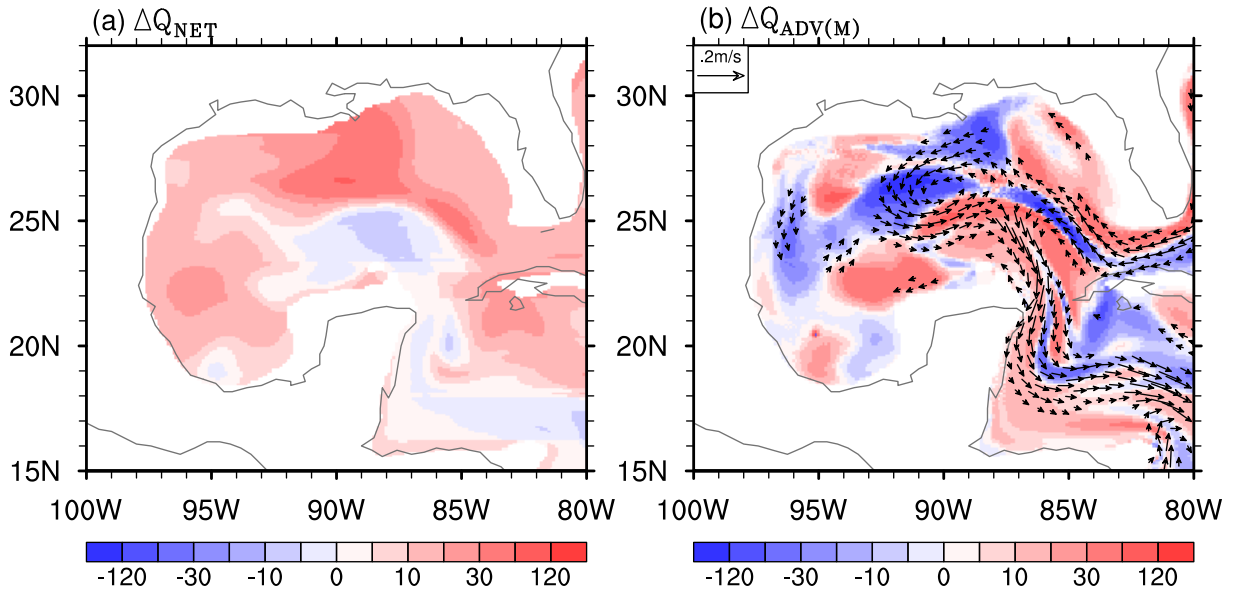


Figure 3. (a) Anomalous (i.e., late 21st century – late 20th century) surface heat flux in the GoM during MAM obtained from EXP_HR. (b) Anomalous (i.e., late 21st century – late 20th century) advective heat flux convergence (colored) and surface current (vector) in the GoM during MAM obtained from EXP_HR. The unit for the heat flux terms is W/m^2 .

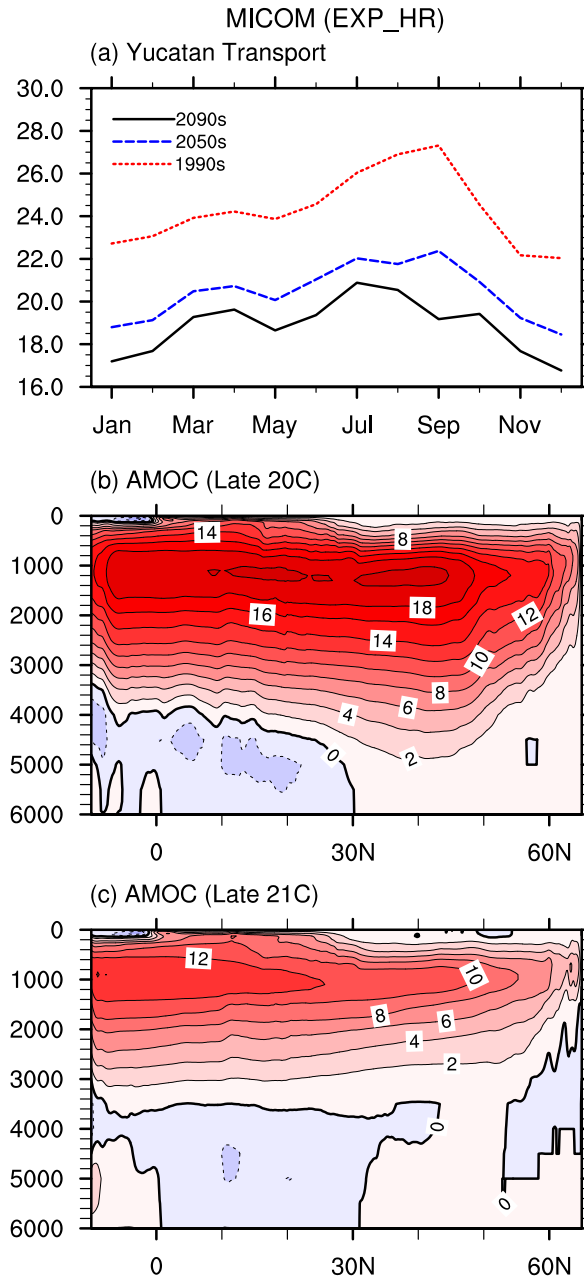


Figure 4. (a) Seasonal cycle of the volume transport (Sv) across the Yucatan Channel for three different periods (the late 20th century, the mid 21st century and the late 21st century) obtained from EXP_HR. Time-averaged Atlantic MOC in (b) the late 20th century and (c) the late 21st century obtained from EXP_HR.

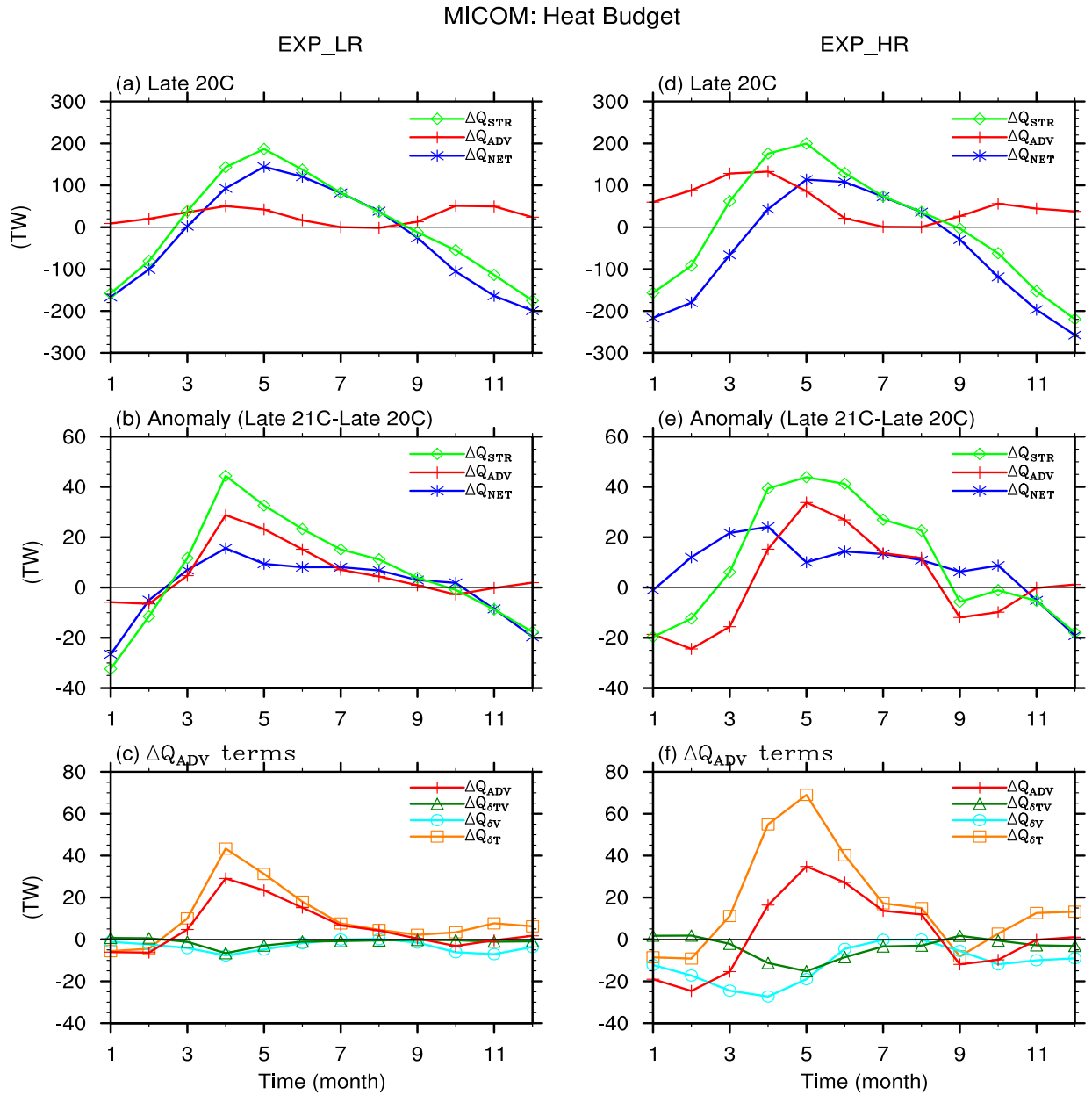


Figure 5. Seasonal cycle of heat budget terms averaged in the GoM (a) for EXP_LR in the late 20th century and (d) EXP_HR in the 20th century. Anomalous (i.e., late 21st century – late 20th century) seasonal cycle of heat budget terms averaged in the GoM (b) for EXP_LR and (e) EXP_HR. Anomalous (i.e., late 21st century – late 20th century) seasonal cycle of advective heat convergence and all the contributing terms ($\Delta Q_{\delta T}$, ΔQ_V and $\Delta Q_{\delta TV}$) averaged in the GoM (c) for EXP_LR and (f) EXP_HR.